

FLOW FIELD AND TOPOLOGICAL ANALYSIS OF HEMISPHERICAL PARACHUTE IN LOW ANGLES OF ATTACK

YIHUA CAO, QIANFU SONG* and ZHUO WU
*School of Aeronautical Science and Engineering,
Beijing University of Aeronautics and Astronautics,
Beijing 100191, China*
**TaiKongs@ase.buaa.edu.cn*

JOHN SHERIDAN
*Department of Mechanical and Aerospace Engineering,
Monash University, VIC 3800, Australia*

Received 2 August 2009
Revised 22 November 2009

For analyzing the flow field and topological structure of hemispherical parachute in low angles of attack, a fluid-structure interaction (FSI) simulation technique is established to decide the shape of the hemispherical parachute during terminal descent. In the fluid simulation, the semi-implicit method for pressure-linked equations consistent (SIMPLEC) algorithm is introduced to solve shear stress transport (SST) k - ω turbulence Navier–Stokes (N–S) Equations. This method is proved to be efficient and stable by the experiment and corresponding numerical simulation. After obtaining the stable shape of the canopy, the parachute in different angles and velocities are considered.

Keywords: Hemispherical parachute; fluid-structure interaction; topological analysis.

1. Introduction

The main research areas of parachute numerical simulation include flow field simulation, structure simulation and fluid-structure interaction (FSI) simulation, among which FSI simulation is the most difficult one. However, because the FSI simulation express the parachute work process more accurately, and could get more reasonable results, it is gradually gaining popularity.

In order to carry out the parachute numerical fluid-structure interaction simulation, much research has been done and many models have been developed recently to solve the dynamics problem of parachute systems simulation. One of the most-used models is the space-time FSI technique. It is based on the deforming-spatial-domain/stabilized space-time (DSD/SST) method,^{1–3} which is a moving-mesh technique. The earliest applications of these space-time FSI techniques included 2D and 3D flow computations.^{1–5} These were followed by the first applica-

tion of the space-time FSI techniques to parachute modeling, reported in Ref. 6 as axisymmetric computation of the inflation of a parachute. Application to parachute modeling with full 3D computations was first reported in Ref. 7, in the context of a parafoil, together with a detailed description of the method and parallel implementation. The same technique was used in Ref. 8 for a detailed 3D computation of a round parachute. These early parachute applications were computed with the block-iterative coupling technique (see Refs. 9 and 10 for the terminology and context). More robust versions of these early block-iterative techniques were introduced in Ref. 9. Also introduced in Ref. 9 were the quasi-direct and direct coupling techniques, which yield more robust algorithms for FSI computations where the structure is light and therefore more sensitive to the variations in the fluid dynamics forces (that is what we have in parachute modeling). The SST FSI technique was applied to a number of parachute simulations, including parachutes with fabric porosity¹⁰ and the ringsail parachutes to be used with NASA's new space vehicle Orion.^{11–13}

This paper mainly concerns the fluid-structure interaction problem of a hemispherical parachute during its terminal descent. Different from the space-time FSI technique, this paper establishes a new numerical simulation technique to deal with the parachute FSI problem on both fluid and structure analysis. In the fluid simulation, the semi-implicit method for pressure-linked equations consistent (SIMPLEC) algorithm is introduced to solve shear stress transport (SST) k - ω turbulence Navier–Stokes (N–S) equations, and an experiment is done to justify the method used in fluid simulation codes in water tunnel. The method is proved to be efficient and stable by the experiment and corresponding numerical simulation. In the structure simulation, the canopy gore centerline and cord line are used to decide canopy shape variation. To couple the fluid and structure codes, the canopy pressure coefficient and shape parameters can be obtained. The results show that the technique could find the final shape of the hemispherical parachute quickly.

The contents of this paper are organized as follows. Section 2 is devoted to the problem statement. The geometric characteristics of the hemispherical parachute model to be simulated will be presented. In Sec. 3, the fluid numerical simulation method and corresponding experiment will be discussed. In Sec. 4, the structure simulation method will be introduced. In Sec. 5, the fluid and structure simulation codes coupling process will be described. Finally, in Sec. 6, for analyzing the parachute flow fields in different states, low angles of attack range of 0° – 15° and different velocities are considered, and the topological structure in typical state is analyzed. The conclusion is given in Sec. 7.

2. Modeling

The geometric parameters of the referred hemispherical parachute in the paper are shown in Table 1, and the hemispherical parachute profile is shown in Fig. 1.

Table 1. The primary parameters of the hemispherical parachute.

Bottom diameter, <i>m</i>	Vent diameter, <i>m</i>	Suspension line, <i>m</i>	Gore number	Angle of attack, degree	Steady velocity, m/s
2	0.2	2.8	8	0–15	6.0

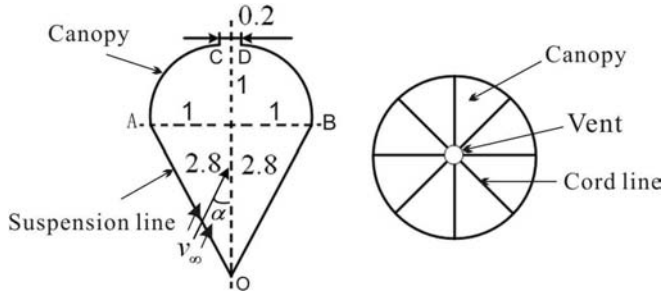


Fig. 1. The hemispherical parachute profile, *m*.

3. Flow Field Simulation

3.1. Governing equations

During the terminal descent of the hemispherical parachute, the surrounding air-flow is considered to be incompressible steady flow, then the Navier–Stokes (N–S) Equations can be written in the form of the flowing two equations:

$$\nabla \cdot u = 0, \tag{1}$$

$$\rho(u \cdot \nabla \cdot u + f) - \nabla \cdot \sigma = 0, \tag{2}$$

where *u*, ρ , *f* and σ are the velocity vector, density, external body force and stress tensor respectively.

There are mainly three methods to solve the N–S equations, including the finite difference method (FDM), finite element method (FEM) and finite volume method (FVM). In the process of solving N–S equations, using the above methods will bring new variables (turbulence viscosity coefficient μ_t , etc.). To overcome this problem, the turbulence model was produced.

This paper uses the semi-implicit method for pressure-linked equations consistent (SIMPLEC) algorithm to solve shear stress transport (SST) *k*– ω turbulence Navier–Stokes (N–S) Equations.

There are two types of calculation grids (plotted by Gridgen software, see Fig. 2) used in this paper. The grid of one gore (Fig. 2(a)) is used for the calculation of the symmetrical flowfield, and the full-sized grid (Fig. 2(b)) is used for the calculation of the non-symmetrical flowfield.

The computational domain of one gore grid is shown in Fig. 3. The inner and outer of the canopy (curved face IJKL) are set to wall boundary conditions. Line AE, plane AEF and plane AEG are set to symmetrical boundary conditions. Plane



Fig. 2. The hemispherical parachute calculation grid.

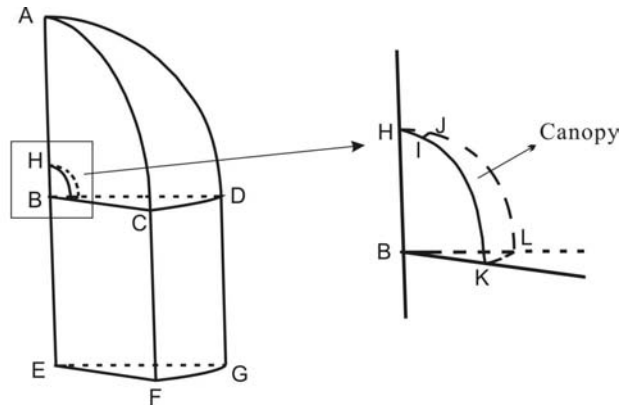


Fig. 3. The computational domain of one gore.

EFG and curved face AFG are set to velocity inlet boundary conditions because the outer boundaries of the computational domain are not affected by the flow over the canopy. In the full-sized grid, the canopy is set to wall boundary conditions, and all outer boundaries of the computational domain are set to velocity inlet boundary conditions.

The main purpose for the flow field simulation in the FSI simulation technique is to calculate the pressure distribution ΔC_p (the pressure coefficient difference between the inner and outer canopy) for structure simulation. ΔC_p is the pressure coefficient C_p difference between the inner and outer surface of the canopy:

$$C_p = \frac{p - p_\infty}{\frac{1}{2}\rho v_\infty^2}, \tag{3}$$

where p is static pressure, v_∞ is the incoming airflow velocity in infinite far field, and p_∞ is the static pressure in infinite far field.

3.2. The SIMPLEC algorithm

The semi-implicit method for pressure-linked equations consistent (SIMPLEC) algorithm¹⁴ was proposed by Van Doormal and Raithby in 1984. It is one of the

improved algorithms of the Semi-Implicit Method for Pressure-Linked Equations (SIMPLE) algorithm¹⁵ which was proposed by Patanker and Spalding in 1972.

The SIMPLEC algorithm could make the calculation convergent more easily. In SIMPLE, the algorithm takes no account of the variance brought by velocity correction of source item which represents the influence brought by velocity correction of neighbor points on that of solution point. Although this simplification in SIMPLE will not change the results' precision, it will result in the calculation to converge slowly. In the SIMPLEC algorithm, there is no simplification, so one coefficient calculation formula is different from the SIMPLE algorithm in the velocity correction equation.

The main steps of the SIMPLEC algorithm are as follows:

- (1) Assume a velocity distribution, marked as u^0, v^0, w^0 . Then calculate the coefficients and constant terms of the discretized momentum equations.
- (2) Assume a pressure field p^* .
- (3) Solve the two momentum equations in turn, obtain u^*, v^*, w^* .
- (4) Solve the pressure correction equation, obtain p' .
- (5) Modify the value of velocity according to p' .
- (6) Use modified velocity to obtain the variable Φ that couples with velocity. If Φ brings no influence to flow field, it should be obtained after flow field converges.
- (7) Use modified velocity to recalculate the coefficients and constant terms of the discretized momentum equations. Use modified pressure field as initial value of the next step of iterative computation.

The main steps of SIMPLEC and SIMPLE¹⁶ algorithms are similar. Detail information can be found in Refs. 14, 15 and other related references.

3.3. Justifying the flow field simulation method

For justifying the flow field simulation method, an experiment was done in a water tunnel at Monash University. As compared with the experiment and the numerical simulation results, the method is proved to be efficient and stable by the experiment and corresponding numerical simulation. The following two figures are one comparison between the experimental (see Fig. 4) and the numerical (see Fig. 5) simulation results. The comparison shows the similarity between the experiment and numerical simulation results, which means that the flow field simulation method is valid and feasible.

4. The Structure Simulation

The structure simulation method is mainly based on the method used in Ref. 17, and one similar method can also be found in Ref. 18.

The basic assumptions are:

- (1) There are no rigidities in both the canopy cloth and cord line.
- (2) There are same strains and stresses in all of the canopy gore and cord line.

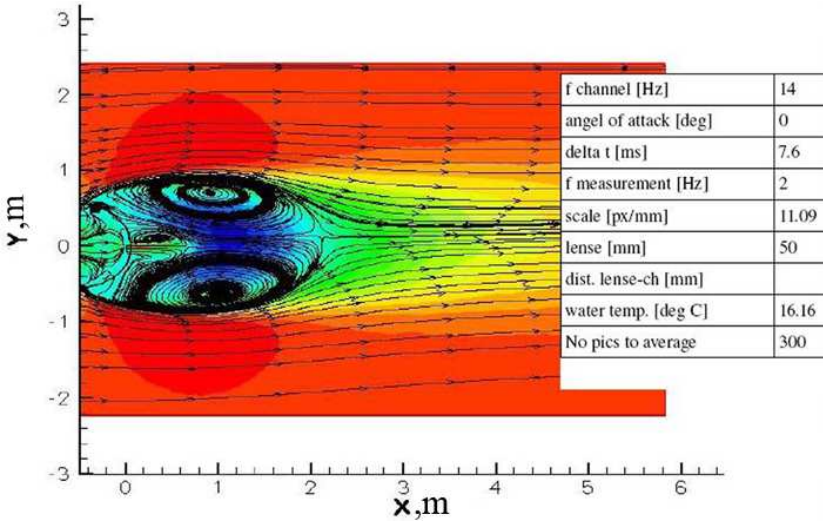


Fig. 4. (Color online) The streamlines and X-velocity contours, $u_\infty = 0.13$ m/s, 14 Hz.

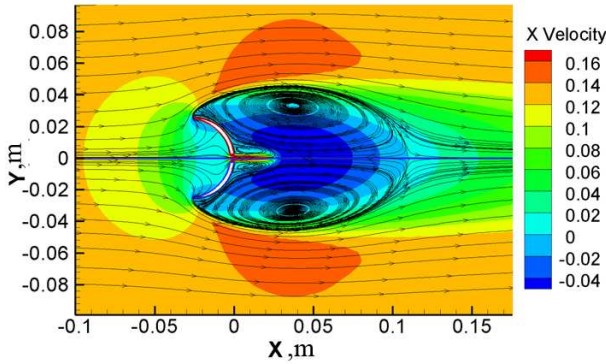


Fig. 5. (Color online) The streamlines and X-velocity contours, $u_\infty = 0.13$ m/s.

- (3) The curve of the intersection boundary between the plane E and canopy gore is one part of a circle.
- (4) The descending velocity is stable.

For the symmetrical characteristic of the hemispherical parachute, one gore of the canopy is used for the structure simulation. Two of the structure model pictures are shown in Fig. 6.

According to the geometrical and physical conditions, the main equations can be obtained, such as the following six differential equations and six algebraic equations:

$$\frac{d\varphi}{dR_f^*} = \frac{1}{\sigma_m^*} \left(1 + \frac{\sigma_m^* - K\sigma_u^*}{E_b^*} \right) \left[\Delta C_p - \frac{\sigma_u^*}{r^*} \cos(\varepsilon - \varphi) \right], \quad (4)$$

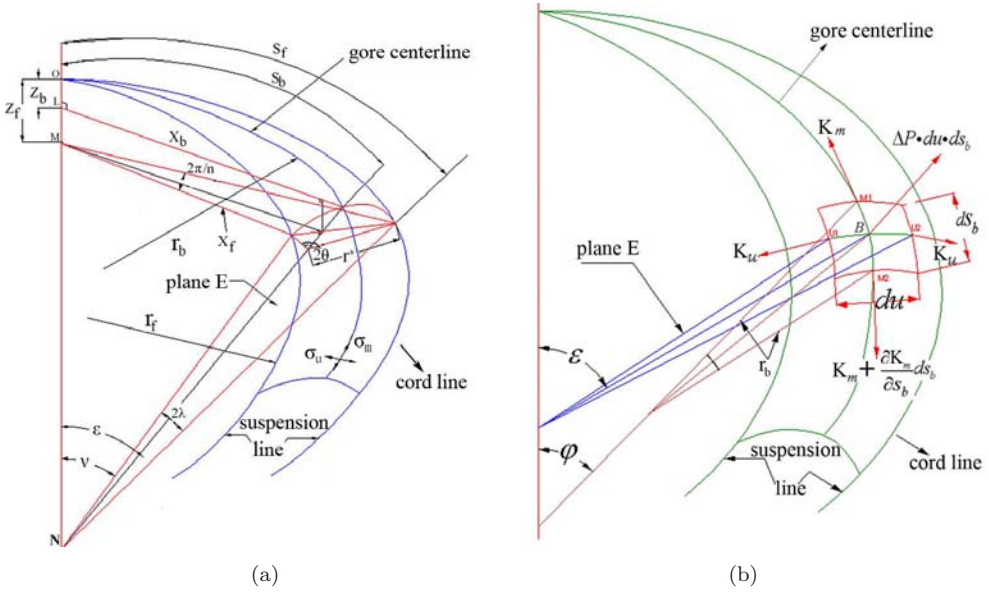


Fig. 6. (Color online) The inflated canopy.

$$\frac{d\sigma_m^*}{dR_f^*} = \frac{\sigma_u^*}{r^*} \left(1 + \frac{\sigma_m^* - K\sigma_u^*}{E_b^*} \right) \sin(\varepsilon - \varphi), \quad (5)$$

$$\frac{dv}{dR_f^*} = \frac{2\sigma_u^*}{T^*} \left(1 + \frac{T^*}{E_f^*} \right) \sin(\theta - \lambda), \quad (6)$$

$$\frac{dT^*}{dR_f^*} = 2\sigma_u^* \left(1 + \frac{T^*}{E_f^*} \right) \cos(\theta - \lambda) \cos \omega, \quad (7)$$

$$\frac{dx_f^*}{dR_f^*} = \left(1 + \frac{T^*}{E_f^*} \right) \cos v, \quad (8)$$

$$\frac{dz_f^*}{dR_f^*} = \left(1 + \frac{T^*}{E_f^*} \right) \sin v, \quad (9)$$

$$r^* \sin \theta = x_f^* \sin \frac{\pi}{N}, \quad (10)$$

$$\theta r^* = \left(1 + \frac{\sigma_u^* - K\sigma_m^*}{E_b^*} \right) \frac{\pi}{N} \sin R_f^*, \quad (11)$$

$$\sigma_u^* = \frac{\Delta C_p r^* T^*}{2\sigma_m^* r^* \sin(\theta - \lambda) + T^* \cos(\varepsilon - \varphi)}, \quad (12)$$

$$\sin \lambda = \sin \frac{\pi}{N} \sin v, \quad (13)$$

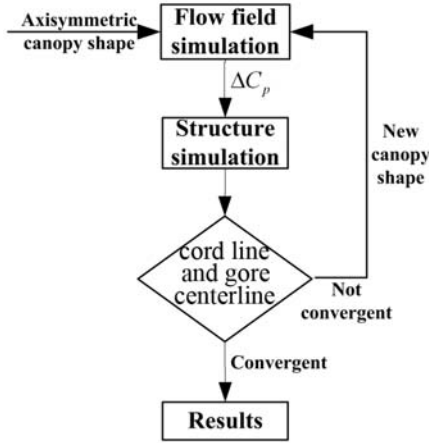


Fig. 7. The FSI simulation technique algorithmic strategy.

$$\sin \varepsilon = \frac{\sin v}{\cos \lambda} \cos \frac{\pi}{N}, \tag{14}$$

$$\sin \omega = \frac{\cos(\pi/N)}{\cos \lambda}. \tag{15}$$

Most of the above equations for hemispherical parachute are similar to the equations in Ref. 17, except for Eqs. (4), (5) and (11), which could be derived from the geometry characteristic of hemispherical parachute.

For more details of the basic structure simulation method, it refer to Refs. 17 and 18.

From the structure simulation codes, the new canopy cord line and gore centerline shape will be obtained, and the new gore of canopy can be plotted out.

5. The Fluid-Structure Interaction Simulation

5.1. The fluid-structure interaction simulation technique

The FSI simulation technique algorithmic strategy for the hemispherical parachute during terminal descent are expressed in Fig. 7.

In the flow field simulation, the canopy shape is supposed to be unchanged. In the structure simulation, the pressure distributions from the flow field simulation are assumed to be unchanged. Actually, both the canopy shape and its surrounding flow have a tiny change during terminal descent. From this sense, there is a simplification for this simulation technique.

The main idea of the fluid-structure interaction simulation technique is to get the canopy pressure distribution ΔC_p (the pressure coefficient difference between the inner and outer canopy) from the flow field simulation codes, then use ΔC_p to calculate the new cord line and gore centerline shape parameters in the structure



Fig. 8. One gore of the canopy.

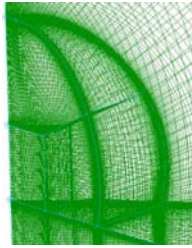


Fig. 9. The calculation grid around the canopy.

simulation codes. If the two lines are convergent, the final canopy shape is obtained. Otherwise, the fluid-structure interaction simulation calculation should be continuously made through using the new canopy shape so as to get the new pressure distribution.

In order to get the stable canopy shape quickly, the FSI simulation technique for the hemispherical parachute during terminal descent takes the axisymmetrical hemispherical canopy shape as the initial shape, because its pressure distribution is more likely to the stable canopy pressure distribution.

5.2. The coupling process and results

In the process of whole fluid-structure interaction simulation, the zero degree angle of attack for the incoming airflow is the basic assumption. Because of the symmetry characteristic of the hemispherical parachute, one gore of the canopy is used for both the flow field simulation and the structure simulation.

The initial one gore canopy shape and its calculation grid around the canopy are shown in Figs. 8 and 9 (plotted by Gridgen software). The canopy thickness is not considered.

Through the flow field simulation, the pressure difference distribution of the gore centerline can be calculated from its inner and outer pressure coefficients. At the beginning and end of the gore centerline, the pressure coefficients equal each other, because the canopy thickness is not considered.

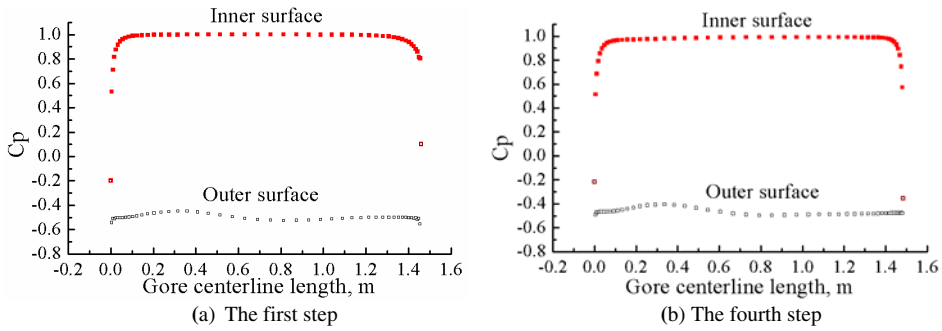


Fig. 10. The inner and outer pressure coefficient along the gore centerline.

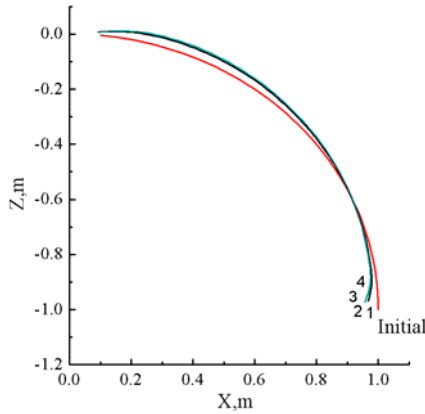


Fig. 11. The variation of gore centerline.

Using the pressure distribution of the gore centerline obtained from the flow field simulation, the structure simulation codes will calculate the new gore centerline and cord line, which could match a new gore shape of the canopy. Likewise, the new gore shape of the canopy could provide a new group of gore centerline pressure distribution for the structure simulation. When the gore centerlines and cord lines calculated from the structure simulation almost do not change any more, the canopy shape is considered to be convergent, and the shape is deemed to be the stable shape of the hemispherical parachute.

After four steps of calculations, the inner and outer pressure coefficients along the gore centerline in the first step and fourth step are shown in Fig. 10. The gore centerline and cord line shape variation are shown in Figs. 11 and 12.

Figures 11 and 12 show that the variation of the gore centerlines and cord lines in steps 2, 3 and 4 are very tiny, so the gore shape is considered to be convergent.

Therefore, the variation of canopy shape during coupling process and the convergent hemispherical parachute structure shape can be drawn in Figs. 13 and 14 (plotted by Rhinoceros software), respectively.

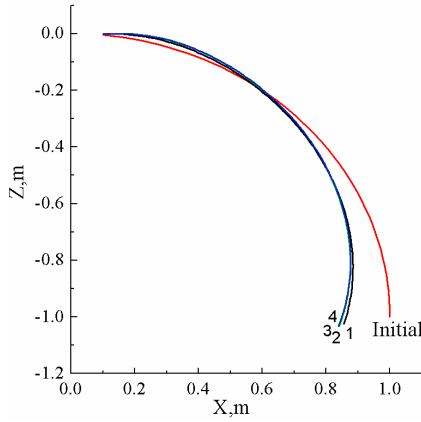


Fig. 12. The variation of cord line.



Fig. 13. The variation of canopy shape during coupling process.



Fig. 14. The convergent hemispherical parachute structure shape.

6. Flow Field and Topological Analysis

Considering the above fluid-structure interaction simulation for zero degree angle of attack at the velocity of 6 m/s during the terminal descent, it is necessary to analyze the flow fields of the hemispherical parachute in other conditions with different angles of attack and velocities. And through the analysis of the topological structure in typical state, the parachute, which is not in an absolutely real stable state during terminal descent, is proved.

6.1. *Different angles of attack*

To analyze the impact of different angles of attack (0° , 5° , 8° , 10° and 15°) on flow pattern in flow field simulation, the streamlines, velocity magnitude and pressure distribution are discussed through using the convergent canopy shape gained from the FSI simulation at 6 m/s velocity. The following figures (Figs. 15–24) are the streamlines, velocity magnitude, and pressure contours in the gore centerline plane at different angles of attack. Among the figures, Figs. 15 and 16 are calculated from one gore of the canopy model; the others are calculated from the full-sized model. Besides, in all the pressure contours figures, the pressures are the relative value referring to 101325 Pa.

From Figs. 15 through 24 it shows that the obvious change is the entire canopy wake zone deviating to the right direction with the increasing of the angle of attack.

There are two big vortexes in the wake flow at zero angle of attack. With the increasing of the angle of attack, the right one becomes smaller and smaller. Although the variation of the left one is not so regular, with the change of its vortex position and size, the maximum minus pressure zone becomes closer to the left outer canopy.

Besides, the change of velocity magnitude in the flow field can be also found in the figures; the maximum velocity magnitude at beyond 10° angle of attack especially becomes higher.

6.2. *Different velocities*

To analyze the different angles of attack, to discuss the impact of different velocities (2 m/s, 4 m/s, 6 m/s, 8 m/s and 10 m/s) on flow pattern, the streamlines, velocity magnitude, and pressure distribution are also discussed, using the convergent canopy shape obtained from the FSI simulation at zero angle of attack in flow field simulation. Figures 25 through 32 are the streamlines, velocity magnitude, and pressure contours in the gore centerline plane at different incoming velocities. The 6 m/s condition figures can be seen in Figs. 15 and 16. All the figures are calculated from the one gore canopy model in flow field simulation. In all the pressure contour figures, the pressures are the relative value referring to 101325 Pa.

From Figs. 15, 16 and 25 through 32, the obvious variation of the velocity magnitude and pressure can be seen with the change of incoming velocity.

There is no vortex in the inner side of the canopy at 2 m/s, but when the velocity is beyond 4 m/s, two small vortexes appear, and the streamline and pressure patterns are almost unchanged.

The above analysis indicates that the topological structure of the canopy in the gore centerline plane is almost unchanged when the velocity is beyond 4 m/s, and it can help the topological analysis for the hemispherical parachute in terminal descent.

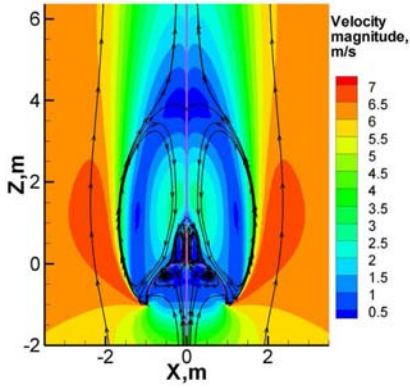


Fig. 15. (Color online) The streamlines and velocity magnitude contours, $\alpha = 0^\circ$.

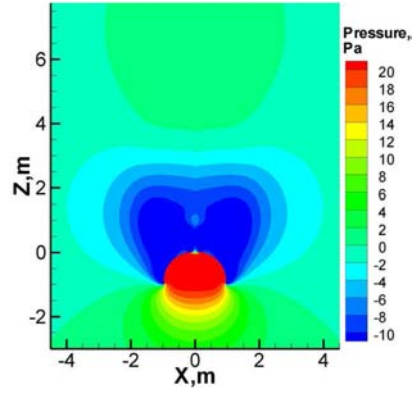


Fig. 16. (Color online) Pressure contours, $\alpha = 0^\circ$.

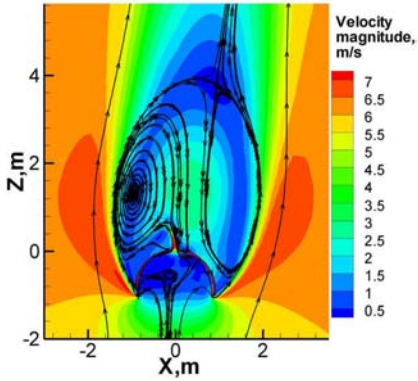


Fig. 17. (Color online) The streamlines and velocity magnitude contours, $\alpha = 5^\circ$.

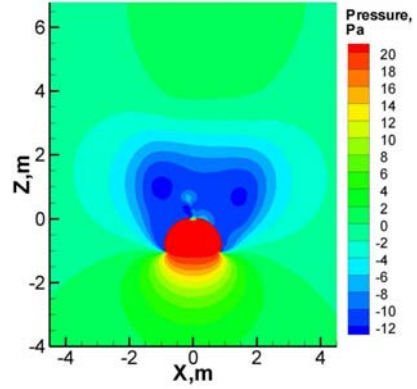


Fig. 18. (Color online) Pressure contours, $\alpha = 5^\circ$.

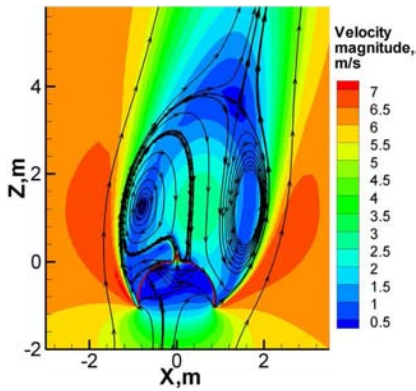


Fig. 19. (Color online) The streamlines and velocity magnitude contours, $\alpha = 8^\circ$.

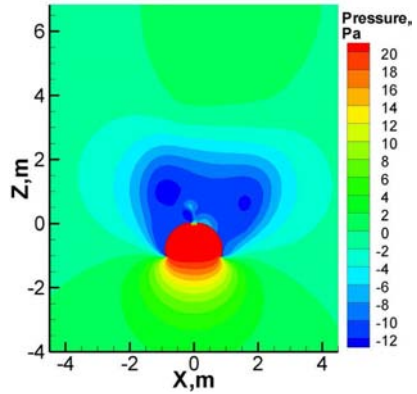


Fig. 20. (Color online) Pressure contours, $\alpha = 8^\circ$.

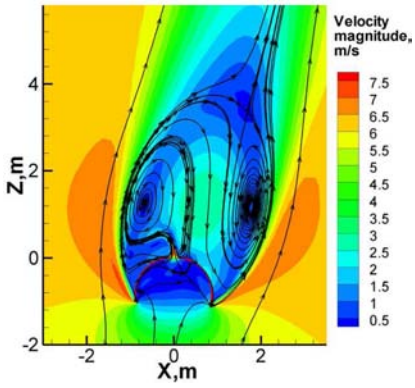


Fig. 21. (Color online) The streamlines and velocity magnitude contours, $\alpha = 10^\circ$.

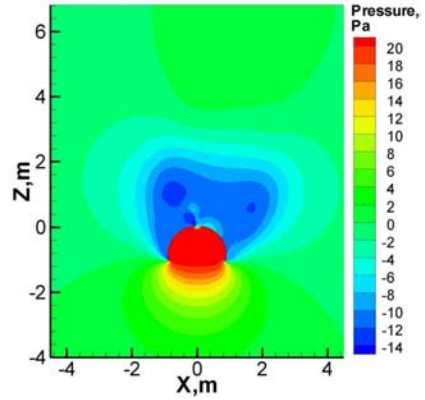


Fig. 22. (Color online) Pressure contours, $\alpha = 10^\circ$.

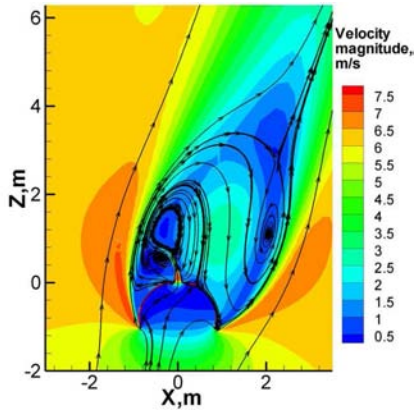


Fig. 23. (Color online) The streamlines and velocity magnitude contours, $\alpha = 15^\circ$.

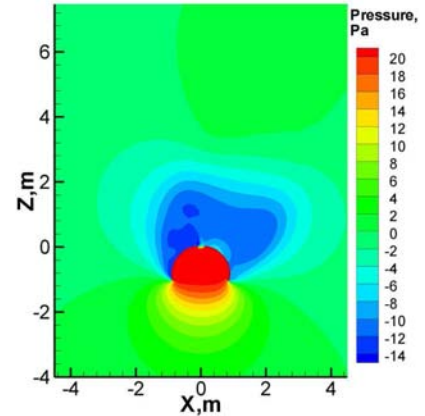


Fig. 24. (Color online) Pressure contours, $\alpha = 15^\circ$.

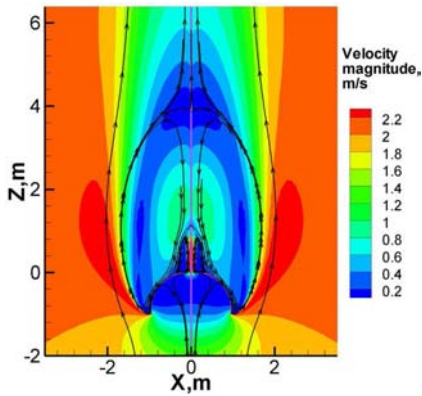


Fig. 25. (Color online) The streamlines and velocity magnitude contours, $u_\infty = 2$ m/s.

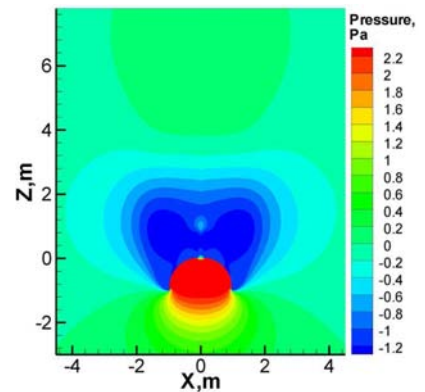


Fig. 26. (Color online) Pressure contours, $u_\infty = 2$ m/s.

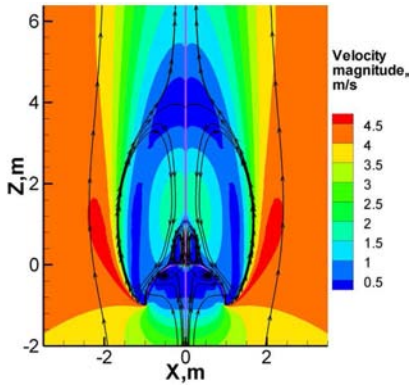


Fig. 27. (Color online) The streamlines and velocity magnitude contours, $u_\infty = 4$ m/s.

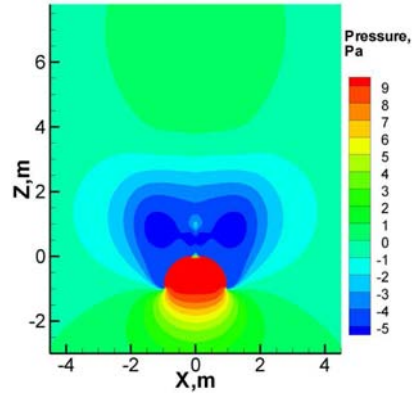


Fig. 28. (Color online) Pressure contours, $u_\infty = 4$ m/s.

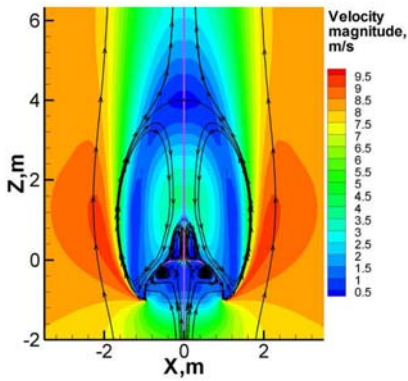


Fig. 29. (Color online) The streamlines and velocity magnitude contours, $u_\infty = 8$ m/s.

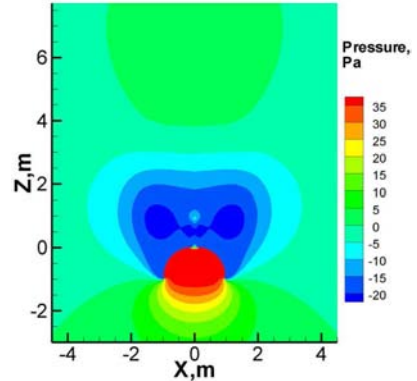


Fig. 30. (Color online) Pressure contours, $u_\infty = 8$ m/s.

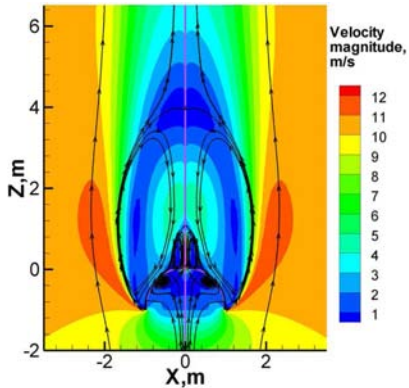


Fig. 31. (Color online) The streamlines and velocity magnitude contours, $u_\infty = 10$ m/s.

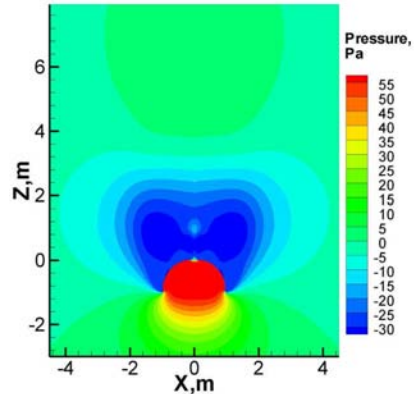


Fig. 32. (Color online) Pressure contours, $u_\infty = 10$ m/s.

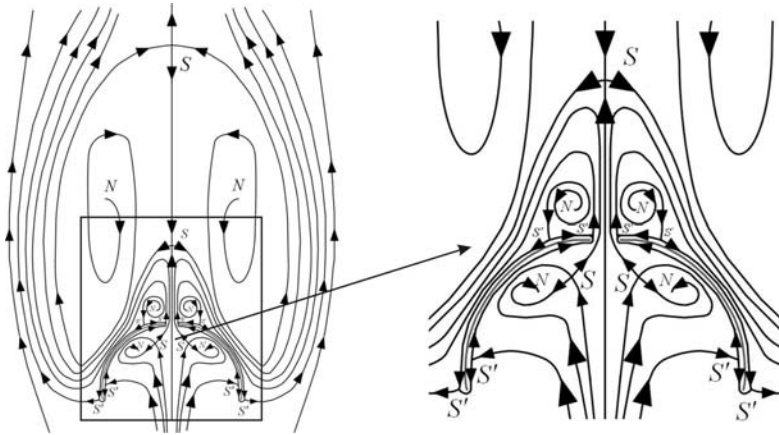


Fig. 33. Topological structure of the stable canopy in gore centerline plane, $u_\infty = 6 \text{ m/s}$, $\alpha = 0^\circ$.

6.3. Topological analysis

The topological theory provides a general tool to rationally analyze the overall qualitative structure of a separated vortex flow, in terms of critical points and their connections on body surface and inside the fluid. It has mainly been applied to steady flow.¹⁹ Therefore, using topological theory to analyze the flow field of the hemispherical parachute in terminal descent, can be an effective method.

According to topological theory, assuming a plane cuts one or more solid bodies in the flow field, the sectional flow on the plane has m isolated finite section planes. The topological rule has the form in Eq. (16):

$$\left(\sum_N + \frac{1}{2} \sum_{N'} \right) - \left(\sum_S + \frac{1}{2} \sum_{S'} \right) = 1 - n, \tag{16}$$

where N, N', S and S' are the node, semi-node, saddle, and semisaddle, respectively; $n = m + 1$.

The topological structure of the stable canopy in gore centerline plane in the typical condition ($u_\infty = 6 \text{ m/s}$, $\alpha = 0^\circ$) is shown in Fig. 33. It contains 4 saddles, 6 nodes, 8 semisaddles, 0 seminodes, and 2 isolate finite section planes. So the topological structure obeys the topological rule in Eq. (16).

The flow field topological structure has strong connection with the flow field. For example, the variation of the Z -velocity along the Z axis in the gore centerline plane ($u_\infty = 6 \text{ m/s}$, $\alpha = 0^\circ$) is shown in Fig. 34. There are two zero Z -velocity points along the Z axis, and thus there are two saddles on the Z axis in the flow field topological structure correspondingly.

In Fig. 33, there are 4 spiral source nodes at the outer side of the canopy and 2 spiral sink nodes at the inner side of the canopy. Reference 18 indicates that if the flow is incompressible, then the structure is unsteady with alternative periodic spiral sink and source, associated with a fluctuating velocity component along the third dimension. So the topological structure in Fig. 33 is unsteady.

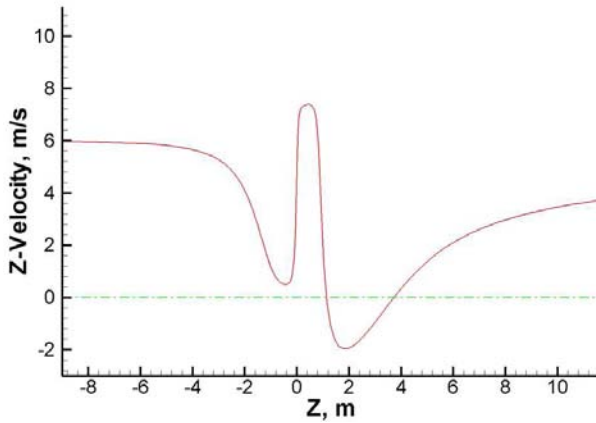


Fig. 34. The variation of the Z -velocity along the Z axis in the gore centerline plane, $u_\infty = 6$ m/s, $\alpha = 0^\circ$.

Therefore, although a theoretical stable canopy can be calculated, the canopy shape will be changed even under a tiny interference. This phenomenon can be used to explain that the parachute during terminal descent is not in an absolutely real stable state, but in a mean stable state.

7. Conclusion

This paper establishes a fluid-structure interaction simulation technique for hemispherical parachute during the terminal descent. In order to analyze the hemispherical parachute flow field more integrally, canopy in different conditions is considered in the flow field analysis. For further understanding, the flow field the topological structure in typical state is analyzed.

The important work of this paper is the introduction of the SIMPLEC algorithm and $k-\omega$ SST turbulence model into the flow field simulation, the accomplishment of the hemispherical parachute structure simulation, the more integrally flow field analysis for fluid-structure interaction (FSI) simulation, and the topological analysis for the flow field of the hemispherical parachute in terminal descent.

Although this FSI simulation technique succeeds in applying for the hemispherical parachute simulation during the terminal descent, there are many extension works needed, such as, considering more influence factors, especially, establishing a new FSI simulation technique which suits the parachute simulation and for analyzing the flow field in the inflation stage, and so on.

Acknowledgment

This work was financially supported by the National Natural Science Foundation of China (Grant No. 10577003).

Nomenclature

- v_∞ = incoming airflow velocity in infinite far field
 α = angle of attack
 u = velocity vector
 ρ = density
 f = external body force
 σ = stress tensor
 C_p = pressure coefficient
 ΔC_p = pressure coefficient difference between the inner and outer canopies
 p = static pressure
 p_∞ = the static pressure in infinite far field
 Plane E = a plane (see Fig. 6)
 φ = an angle between the canopy axis and the normal line of gore centerline
 R_f^* = dimensionless length of apex point of the cord line to the point on itself in unstretched gore state
 σ_m^*, σ_u^* = dimensionless stress in canopy fabric in the longitudinal and latitudinal directions
 K = shrink factor of canopy material
 r^* = dimensionless bulge radius of the canopy
 T^* = dimensionless force in cord line
 x_f^*, z_f^* = dimensionless x and z coordinates of cord line in cylindrical coordinates
 E_b, E_f = dimensionless elasticity modulus of canopy fabric and cord line
 $v, \theta, \lambda, \varepsilon$ = angles (see Fig. 6)
 N = number of gores
 ω = the half angle between two contiguous plane E
 N, N' = node and seminode
 S, S' = saddle and semisaddle

References

1. T. E. Tezduyar, *Adv. Appl. Mech.* **28** (1992) 1–44.
2. T. E. Tezduyar, M. Behr and J. Liou, *Comput. Meth. Appl. Mech. Eng.* **94** (1994) 339–351.
3. T. E. Tezduyar, M. Behr, S. Mittal and J. Liou, *Comput. Meth. Appl. Mech. Eng.* **94** (1992) 353–371.
4. S. Mittal and T. E. Tezduyar, *Int. J. Numer. Meth. Fluids* **15** (1992) 1073–1118.
5. S. Mittal and T. E. Tezduyar, *Int. J. Numer. Meth. Fluids* **21** (1995) 933–953.
6. K. Stein, R. Benney, V. Kalro, A. A. Johnson and T. E. Tezduyar, Parallel computation of parachute fluid-structure interactions, in *Proc. 14th AIAA Aerodyn. Decel. Tech. Conf.*, San Francisco, AIAA-97-1505, 1997.
7. V. Kalro and T. E. Tezduyar, *Comput. Meth. Appl. Mech. Eng.* **190** (2000) 321–332.
8. K. Stein, R. Benney, V. Kalro, T. E. Tezduyar, J. Leonard and M. Accorsi, *Comput. Meth. Appl. Mech. Eng.* **190** (2000) 373–386.
9. T. E. Tezduyar, S. Sathe, R. Keedy and K. Stein, *Comput. Meth. Appl. Mech. Eng.* **195** (2006) 2002–2027.

10. T. E. Tezduyar and S. Sathe, *Int. J. Numer. Meth. Fluids* **54** (2007) 855–900.
11. T. E. Tezduyar, S. Sathe, J. Pausewang, M. Schwaab, J. Crabtree and J. Christopher, Air-fabric interaction modeling with the stabilized space-time FSI technique, in *Proc. 3rd Asian-Pacific Congr. Comput. Mech.*, [CD-Rom], Kyoto, Japan, 2007.
12. T. E. Tezduyar, S. Sathe, J. Pausewang, M. Schwaab, J. Christopher and J. Crabtree, *Comput. Mech.*, published online, March 2008, DOI:10.1007/s00466-008-0261-7.
13. T. E. Tezduyar, S. Sathe, J. Pausewang, M. Schwaab, J. Christopher and J. Crabtree, *Comput. Mech.*, published online (2008), DOI:10.1007/s00466-008-0260-8.
14. J. P. Van Dormal and G. G. Raithby, *Numer. Heat Transf.* **7** (1984) 147–163.
15. S. V. Patanker and D. B. Spalding, *Int. J. Heat Mass Transf.* **15** (1972) 1789–1806.
16. Y. H. Cao, K. Wang, Z. W. Yu and X. Pan, Numerical simulation of parachute fluid-structure interaction and flow field analysis, in *19th AIAA Aerodyn. Decel. Syst. Technol. Conf.*, Williamsburg, AIAA-2007-2573.
17. L. C. Zhu, *Landing Technol.* **1** (1983) 143–177 (in Chinese); translated from the paper titled as *Angenäherter Berechnung der Kräfte, Spannungen und Form des Ebenen Rundkappen-Fallschirms im gefüllten Zustand*, DLR(FB) Q(W) 0860, pp. 71–98.
18. H. G. Heinrich and L. R. Jamison, *Parachute Stress Analysis During Inflation and at Steady State*, AIAA Entry Technology, AIAA-1964-1306.
19. J. Z. Wu, H. Y. Ma and M. D. Zhou, *Vorticity and Vortex Dynamics* (Springer, Berlin, 2006), pp. 323–382.